High-frequency gravitational waves detection based on cubic resonant cavities in the microwave frequency range

Pablo Navarro [1], <u>Benito Gimeno</u> [2], Juan Monzó [1],

Alejandro Díaz-Morcillo [1], Diego Blas [3] [4]

(1) Department of Information and Communications Technologies, Technical University of Cartagena, Murcia, Spain

(2) Instituto de Física Corpuscular (IFIC), CSIC-University of Valencia, Spain

(3) Institut de Física d'Altes Energies (IFAE), The Barcelona Institute of Science and Technology, Spain

(4) Institució Catalana de Recerca i Estudis Avançats (ICREA), Barcelona, Spain

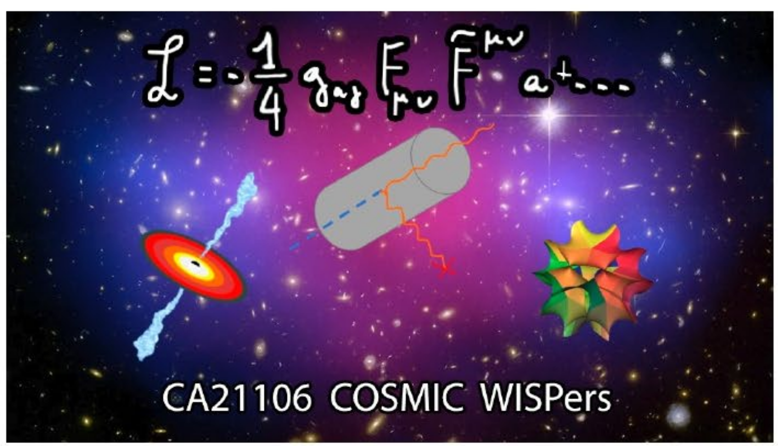

Funded by the European Union

INDEX

INDEX

Introduction

- Gravitational Waves (GWs) are 'ripples' in space-time caused by some of the most violent and energetic processes in the Universe.
- GWs travel at speed of light in vacuum: c = 299792458 m/s
- GWs were first speculated by Henry Poincaré in 1905.
- Albert Einstein predicted the existence of GWs in 1916 in his General Theory of Relativity.

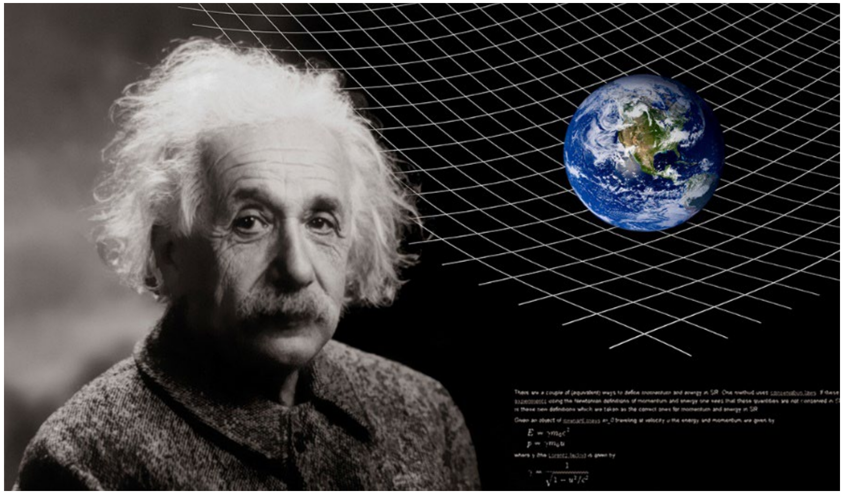

- The first GW was discovered in the LIGO facility (USA) based on an optical interferometer in September 14, 2015 at a frequency ~ 1 kHz

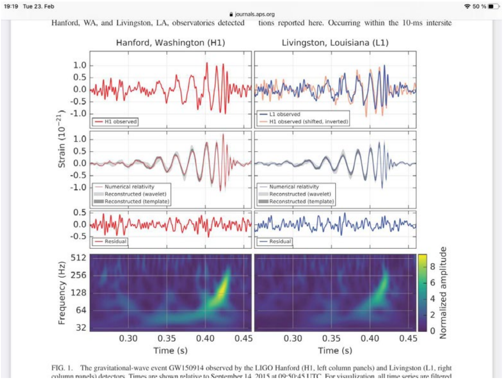

Space resolution of this experiment is 10^{-19} m (10.000 times smaller than the size of a proton)

Introduction

- The <u>LIGO-Virgo collaboration</u> is formed by two optical Michelson interferometers placed in USA (LIGO) and one in Italy (VIRGO).

Aerial views of the LIGO Hanford operated by CALTECH (Washington State, USA) and LIGO Livingston operated by MIT (Luisiana State, USA) interferometers. The arms length is 4 km.

Aerial view of the Virgo interferometer operated by CNRS and INFN (Cascina, near Pisa, Italy). <u>European Gravitational Observatory (EGO)</u> is an European consortium which controls Virgo. The arms length is 3 km.

Introduction

- Several GWs detections have been performed in the last years by the LIGO-Virgo collaboration:

1. GW200105 & GW200115 (First confirmed neutron star-black hole mergers.)
2. GW190521
3. GW190814
4. GW190412
5. GW190425
6. GW170608
7. GW170817 (First binary neutron star detection)
8. GW170814
9. GW170104
10. GW151226
11. GW150914 (First detection)

- GWs are transverse waves with two polarizations states:

CROSS (x)

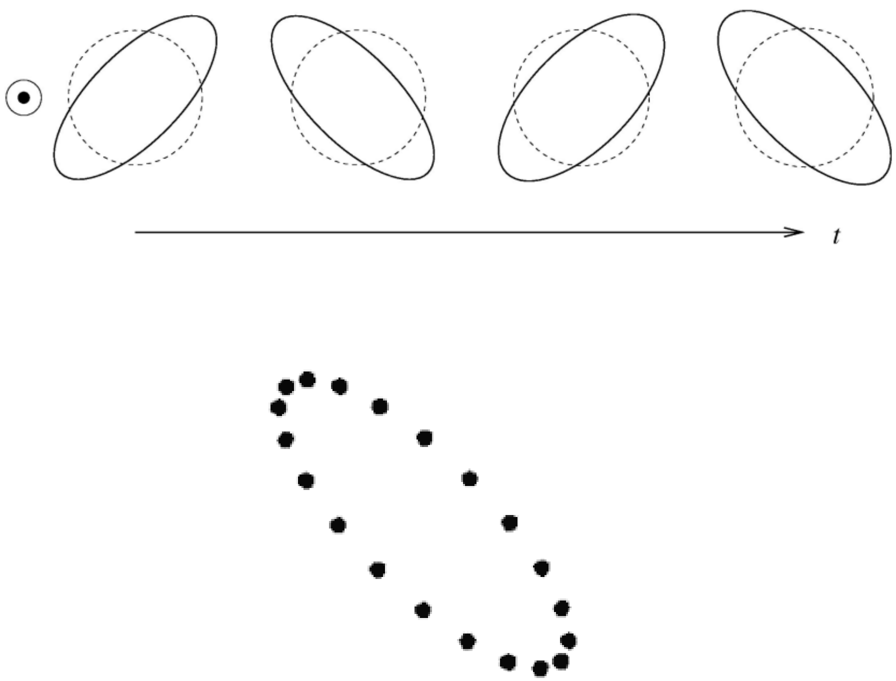

PLUS (+)

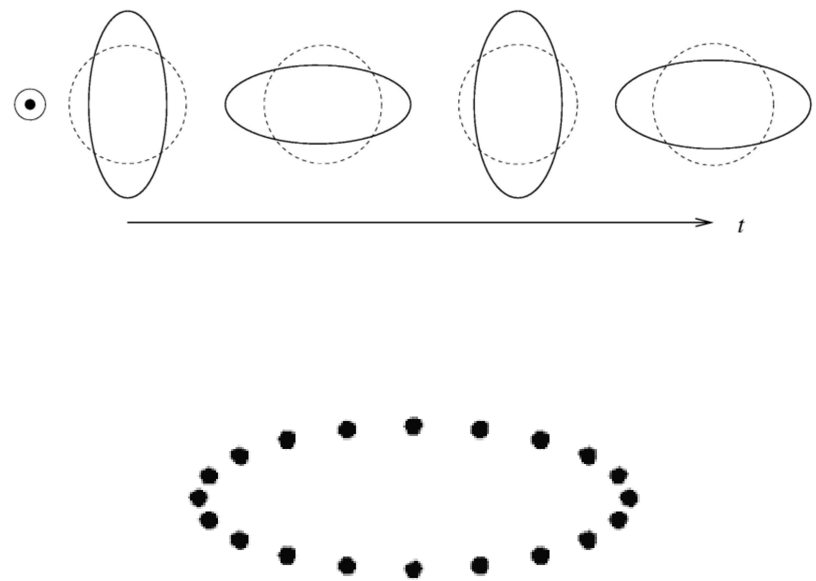

INDEX

Sources of gravitational waves

- There are basically four sources for the generation of GWs:

(1) Continuous GWs are produced by systems that have a well-defined frequency, as binary sytems of stars or black holes orbiting each other (long before merger), or a single star quickly rotating about its axis. These sources are expected to produce comparatively weak GWs since they evolve over longer periods of time and are usually less catastrophic than sources producing inspiral or burst gravitational waves.

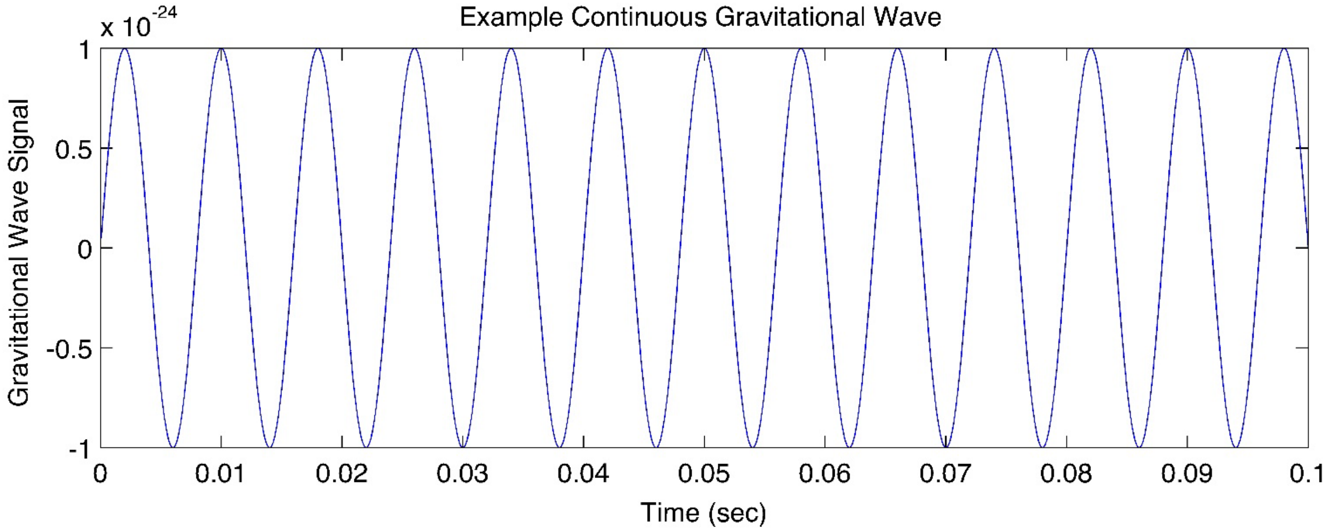

Sources of gravitational waves

(2) Inspiral GWs are generated during the end-of-life stage of binary systems where the two objects merge into one. These systems are usually two neutron stars, two black holes, or a neutron star and a black hole whose orbits have degraded to the point that the two masses are about to coalesce. As the two masses rotate around each other, their orbital distances decrease and their speeds increase. This causes the frequency of the gravitational waves to increase until the moment of coalescence.

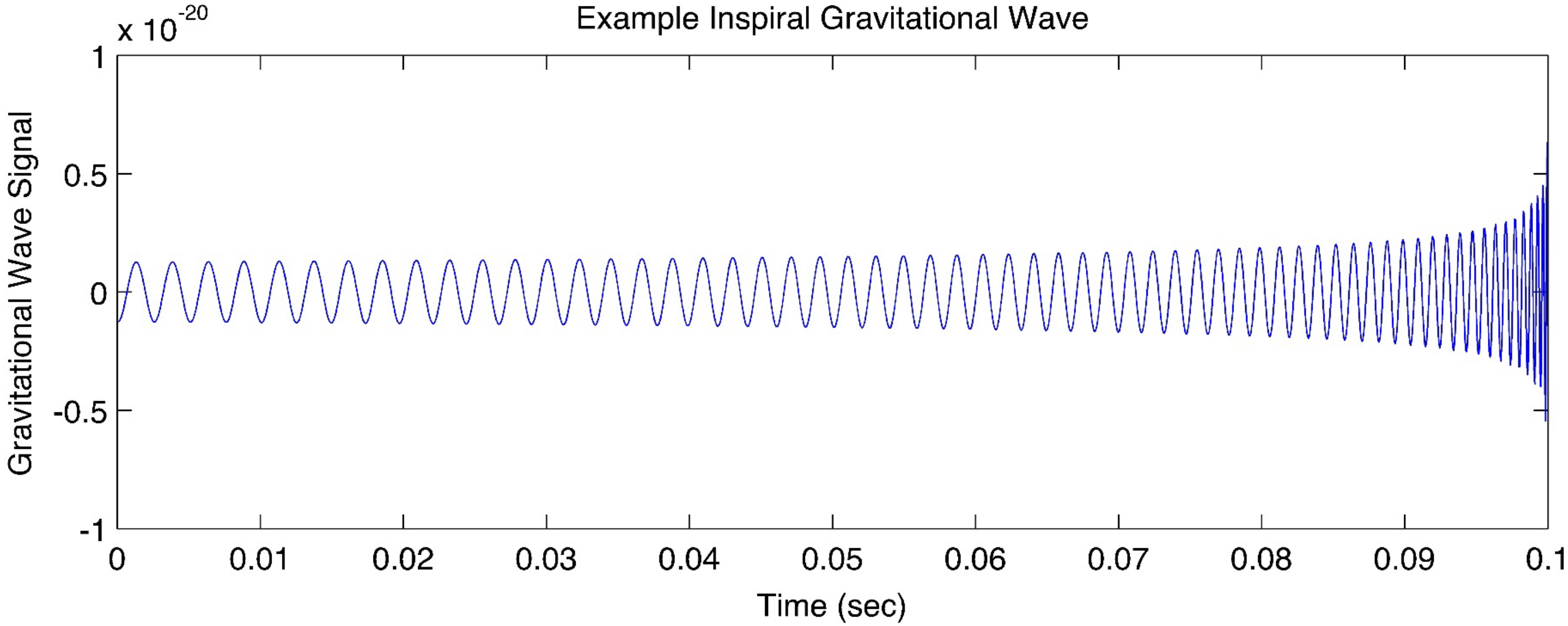

Sources of gravitational waves

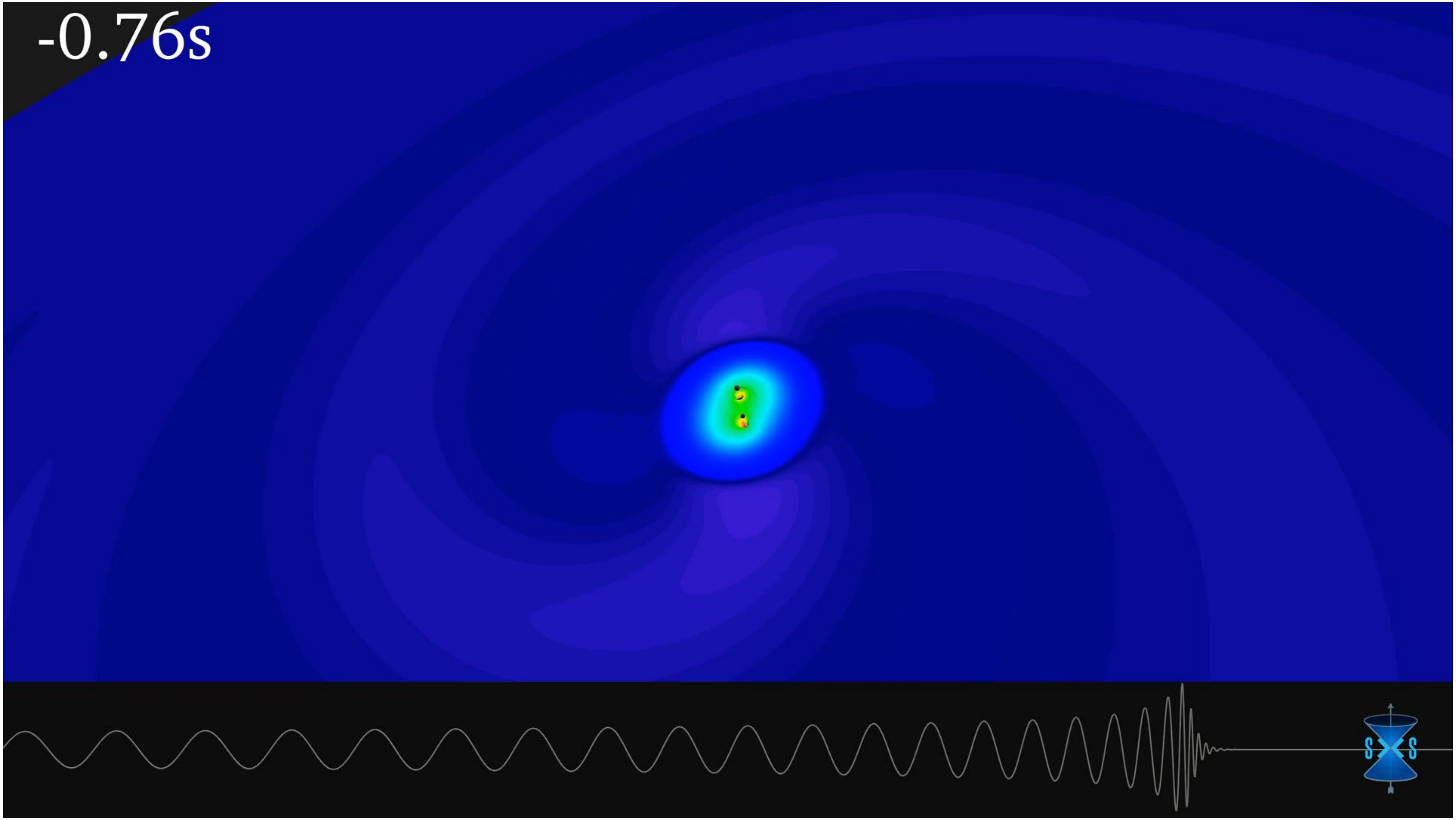

Sources of gravitational waves

(3) Burst GWs come from short-duration cosmological events. In burst GWs we are expecting the unexpected. There are hypotheses that some systems such as supernovae or gamma ray bursts may produce burst GWs, but too little is known about the details of these systems to anticipate the form these waves will have.

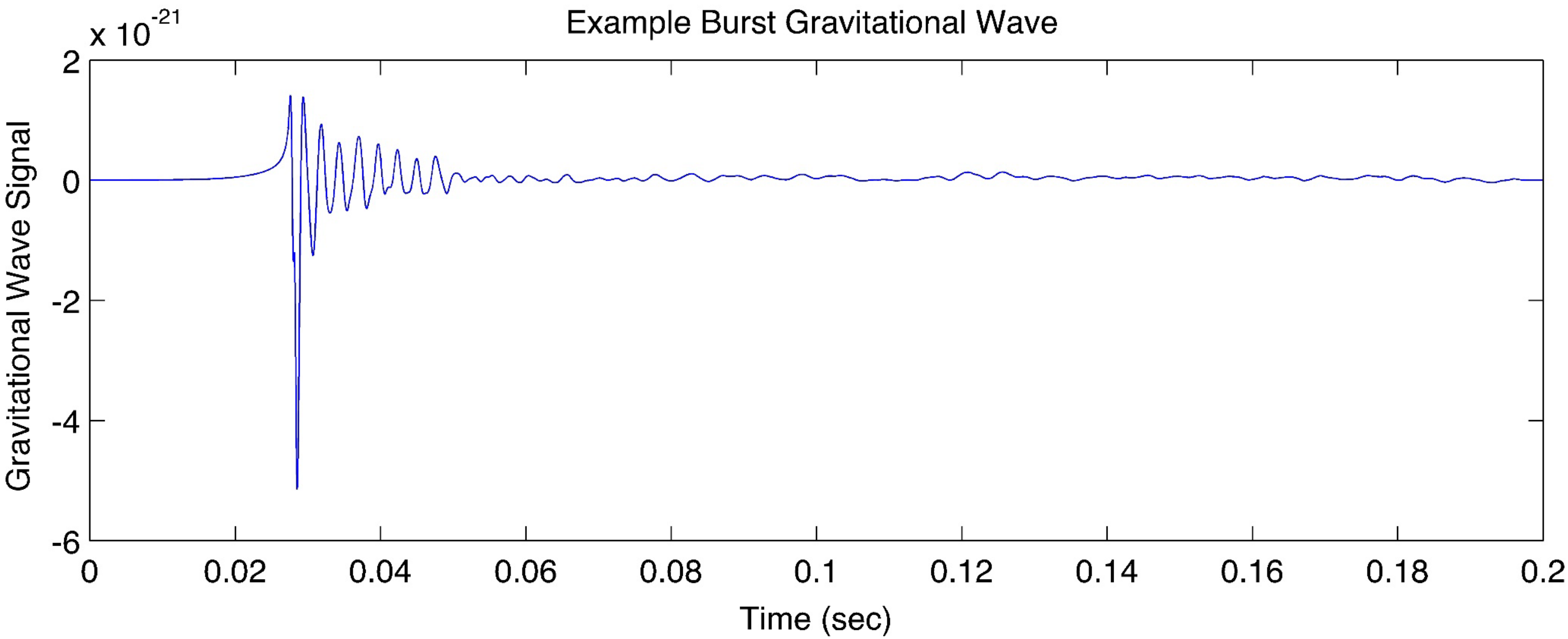

Sources of gravitational waves

(4) Stochastic GWs are the relic GWs from the early evolution of the Universe. Much like the Cosmic Micro-wave Background (CMB), which is likely to be the leftover light from the Big Bang, these GWs arise from a large number of random, independent events as many simultaneous inspirals, bursts, or continuous signals combining to create a cosmic gravitational wave background. The Big Bang is expected to be a prime candidate for the production of the many random processes needed to generate stochastic gravitational waves (and the CMB), and therefore may carry information about the origin and history of the Universe.

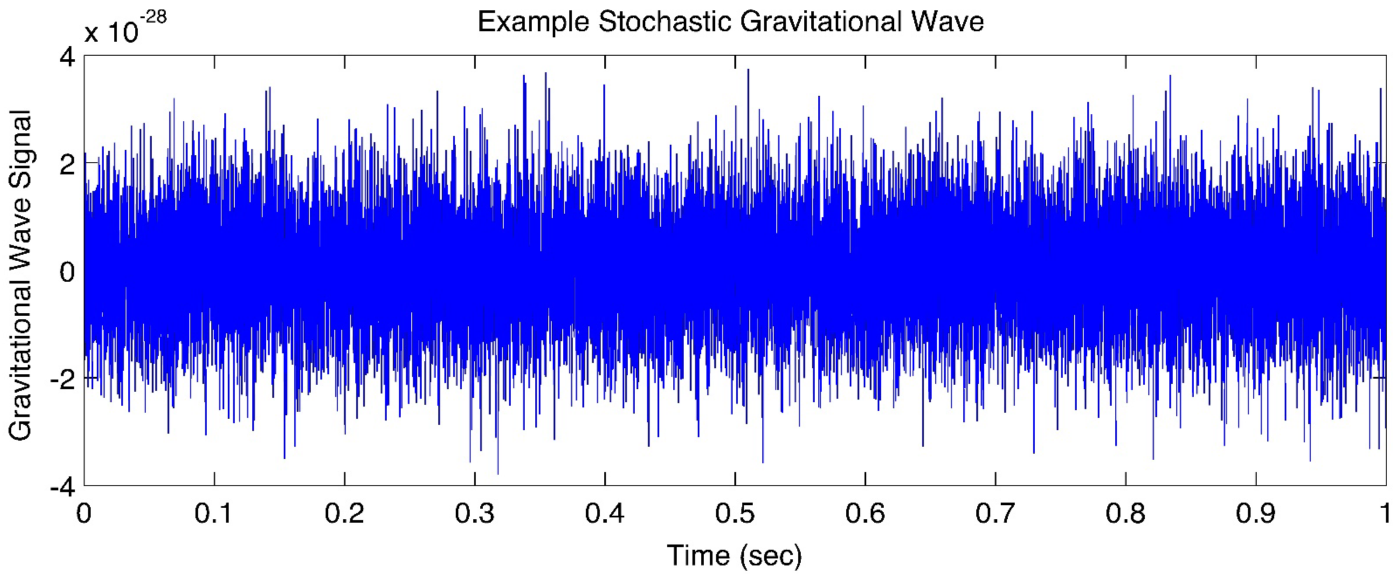

INDEX

Detection of gravitational waves

- Detection of the High-Frequency GWs: based on the **inverse Gertsenhstein effect**

SOVIET PHYSICS JETP VOLUME 14, NUMBER 1 JANUARY, 1962

WAVE RESONANCE OF LIGHT AND GRAVITIONAL WAVES

M. E. GERTSENSHTEĬN

Submitted to JETP editor July 29, 1960

J. Exptl. Theoret. Phys. (U.S.S.R.) **41**, 113-114 (July, 1961)

The energy of gravitational waves excited during the propagation of light in a constant magnetic or electric field is estimated.

SOVIET PHYSICS JETP VOLUME 16, NUMBER 2 FEBRUARY, 1963

ON THE DETECTION OF LOW FREQUENCY GRAVITATIONAL WAVES

M. E. GERTSENSHTEĬN and V. I. PUSTOVOĬT

Submitted to JETP editor March 3, 1962

J. Exptl. Theoret. Phys. (U.S.S.R.) 43, 605-607 (August, 1962)

It is shown that the sensitivity of the electromechanical experiments for detecting gravitational waves by means of piezocrystals is ten orders of magnitude worse than that estimated by Weber.[1] In the low frequency range it should be possible to detect gravitational waves by the shift of the bands in an optical interferometer. The sensitivity of this method is investigated.

Detection of gravitational waves

- The conversion of GWs into electromagnetic waves is a classical process: the propagation of a GW in a region with a very intense static magnetic field generates a perturbation of space-time creating an <u>electromagnetic wave</u> by the Faraday-Lenz induction law:

$$\nabla \times \vec{E} = -\frac{\partial \vec{B}}{\partial t} \quad \Rightarrow \quad \nabla \times \vec{B} = \mu_0 \, \varepsilon_0 \, \frac{\partial \vec{E}}{\partial t}$$

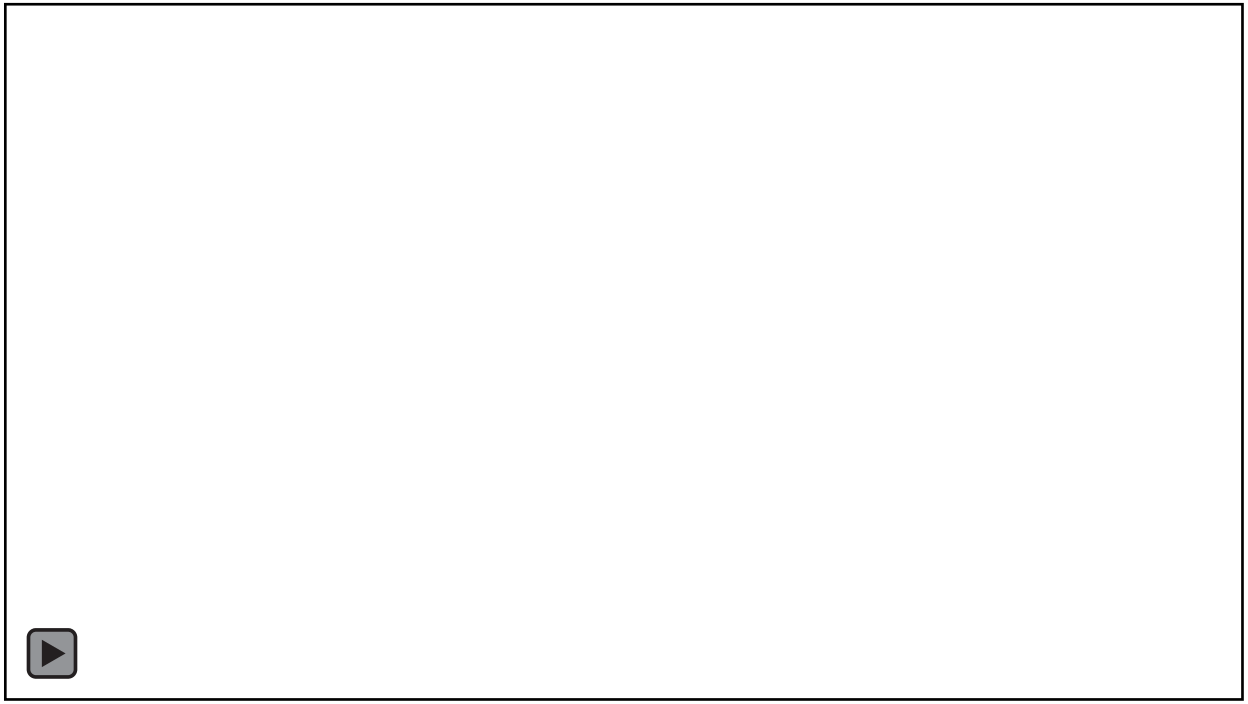

Detection of gravitational waves

- Inverse Primakoff effect: this process is strictly analogous to axion-photon conversion.

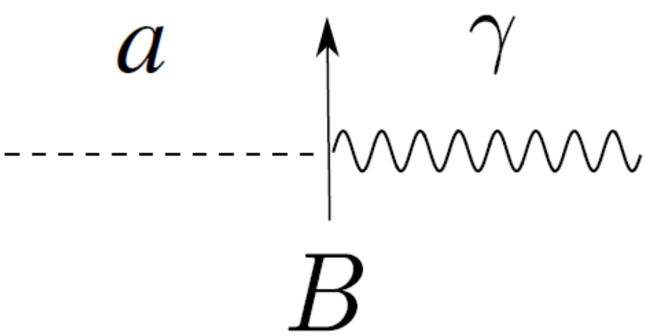

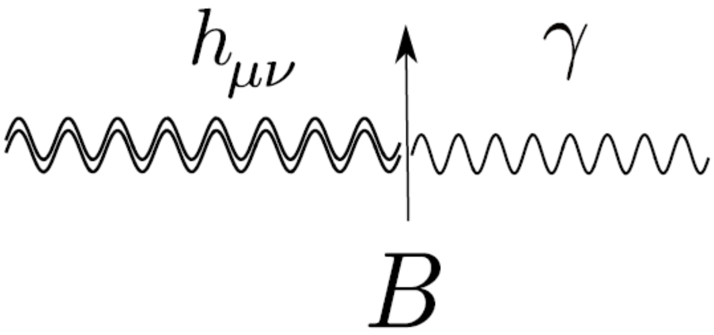

- Ideas and techniques developed for dark matter axions search be adapted to GWs:

Detecting High-Frequency Gravitational Waves with Microwave Cavities

Asher Berlin,[1,2,3] Diego Blas,[4,5] Raffaele Tito D'Agnolo,[6] Sebastian A. R. Ellis,[7,6] Roni Harnik,[2,3] Yonatan Kahn,[8,9,3] and Jan Schütte-Engel[8,9,3]

See also Herman, Füzfa, Lehoucq, Clesse, 2012.12189

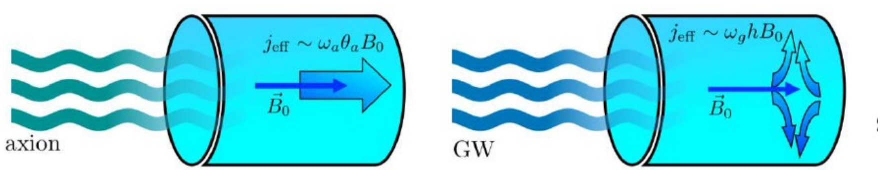

"Detecting high-frequency gravitational waves with microwave cavities", Asher Berlin et al., Physical Review D, **105**, 116011 (2022), pp 1-23

INDEX

The system GW-EM fields: induced current

- From a mathematical point of view, the description of a GW is expressed as a perturbation of an Euclidean local space-time region (without curvature) in terms of the GW field tensor $h_{\mu\nu}$,

$$g_{\mu\nu} = \eta_{\mu\nu} + \varepsilon\, h_{\mu\nu} \;;\; \varepsilon << 1 \;;\; \eta_{\mu\nu} = \begin{pmatrix} -1 & 0 & 0 & 0 \\ 0 & +1 & 0 & 0 \\ 0 & 0 & +1 & 0 \\ 0 & 0 & 0 & +1 \end{pmatrix}$$

where $g_{\mu\nu}$ is the Minkowski metric tensor. This means that the GW represents a perturbation of the conventional space-time.

The system GW-EM fields: induced current

- The calculation of the GW tensor $h_{\mu\nu}$ is performed with the Theory of General Relativity (c=1 in this slide):

$$\mathrm{i} = \sqrt{-1} \qquad h = \eta^{\mu\nu} h_{\mu\nu}$$

$$\boxed{F(x) = \frac{e^{-\mathrm{i}\,x} - 1 + \mathrm{i}\,x}{x^2}}$$

$$U_i = \epsilon_{ijk} V_j \hat{k}_k$$

Non linear behaviour !!

$$h_{ij}^{\mathrm{TT}} = \left[(\mathrm{U}_i \mathrm{U}_j - \mathrm{V}_i \mathrm{V}_j)\, h^+ + (\mathrm{U}_i \mathrm{V}_j + \mathrm{V}_i \mathrm{U}_j)\, h^\times \right] \frac{e^{\mathrm{i}(\omega t - \vec{k}\cdot\vec{r})}}{\sqrt{2}},$$

$$h_{00} = \omega^2 F(\vec{k}\cdot\vec{r})\, \vec{b}\cdot\vec{r}, \qquad b_j \equiv r_i h_{ij}^{\mathrm{TT}}\big|_{\vec{r}=\vec{0}},$$

$$h_{0i} = \frac{1}{2}\omega^2 \left[F(\vec{k}\cdot\vec{r}) + \mathrm{i}F'(\vec{k}\cdot\vec{r}) \right] \left(\hat{k}\cdot\vec{r}\, b_i - \vec{b}\cdot\vec{r}\, \hat{k}_i \right),$$

$$h_{ij} = \mathrm{i}\omega^2 F'(\vec{k}\cdot\vec{r}) \left(||\vec{r}||^2 h_{ij}^{\mathrm{TT}}\big|_{\vec{r}=\vec{0}} + \vec{b}\cdot\vec{r}\,\delta_{ij} - b_i r_j - b_j r_i \right),$$

The system GW-EM fields: induced current

- The presence of an external electromagnetic field (E_i and B_i) acts as a source term to classical Maxwell's equations, effectively inducing an **equivalent electric current density**:

$$
\left.
\begin{aligned}
P_i &= -h_{ij}E_j + \frac{1}{2}hE_i + h_{00}E_i - \epsilon_{ijk}h_{0j}B_k, \\
\tilde{M}_i &= -h_{ij}B_j - \frac{1}{2}hB_i + h_{jj}B_i + \epsilon_{ijk}h_{0j}E_k,
\end{aligned}
\right\} \Rightarrow
$$

$$
\boxed{\partial_\nu F^{\mu\nu} = j^\mu_{\text{eff}} = \left(-\nabla \cdot \vec{P}, \nabla \times \vec{\tilde{M}} + \partial_t \vec{P}\right),}
$$

- In our case: $E_x = E_y = E_z = 0$, and $B_x = B_y = 0$, B_z = constant and uniform.

The system GW-EM fields: induced current

- The analytical expressions of the **equivalent electric current density** in the XZ and YZ planes are very complex (only the Y components are presented):

$$
\begin{gathered}
j_{+,y}^{XZ} = \frac{1}{32\sqrt{2}k(z\cos\theta + x\sin\theta)^4} e^{-ikt}[16kx^3 - 12e^{ik(z\cos\theta+x\sin\theta)}kx^3 - 16kx^2 - \\
-32e^{ik(z\cos\theta+x\sin\theta)}kxy^2 - 6k^3x^3y^2 + 16kxz^2 - 12e^{ik(z\cos\theta+x\sin\theta)}kxz^2 - \\
-6k^3xy^2z^2 + 8ixz(10 + k^2(x^2+y^2+z^2) + 2e^{ik(z\cos\theta+x\sin\theta)} \cdot \\
\cdot(-5 + k^2(x^2+z^2))) \cos\theta - 8kx(-2(1 + 2^{ik(z\cos\theta+x\sin\theta)})y^2 + \\
+z^2(2 + 8e^{ik(z\cos\theta+x\sin\theta)} + k^2z^2) + x^2(2 - 2e^{ik(z\cos\theta+x\sin\theta)} + k^2(-y^2+z^2))) \cos 2\theta - \\
-16ikxz\cos 3\theta + 16ie^{ik(z\cos\theta+x\sin\theta)}xz\cos 3\theta - 4ik^2x^3z\cos 3\theta - \\
-24ie^{ik(z\cos\theta+x\sin\theta)}k^2x^3z\cos 4\theta - \\
-8ik^2xy^2z\cos 3\theta + 20ik^2xz^3\cos 3\theta - 8ie^{ik(z\cos\theta+x\sin\theta)}k^2xz^3\cos 3\theta - \\
-4e^{ik(z\cos\theta+x\sin\theta)}kx^3\cos 4\theta - 2k^3x^3y^2\cos 4\theta + \\
+12e^{ik(z\cos\theta+x\sin\theta)}kxz^2\cos 4\theta + 8k^3x^3z^2\cos 4\theta + 6k^3xy^2z^2\cos 4\theta - 8k^3xz^4\cos 4\theta - \\
-4ik^2x^3z\cos 5\theta + 8ie^{ik(z\cos\theta+x\sin\theta)}k^2x^3z\cos 5\theta + 4ik^2xz^3\cos 5\theta - \\
-8ie^{ik(z\cos\theta+x\sin\theta)}k^2xz^3\cos 5\theta - 8ik^2\sin\theta + \\
+8ie^{ik(z\cos\theta+x\sin\theta)}x^2\sin\theta + 2ik^2x^4\sin\theta + \\
+20ie^{ik(z\cos\theta+x\sin\theta)}k^2x^4\sin\theta + 96iy^2\sin\theta - \\
-96ie^{ik(z\cos\theta+x\sin\theta)}y^2\sin\theta + 12ik^2x^2y^2\sin\theta - 88iz^2\sin\theta + \\
+88ie^{ik(z\cos\theta+x\sin\theta)}z^2\sin\theta - 4ik^2x^2z^2\sin\theta + \\
+24ie^{ik(z\cos\theta+x\sin\theta)}k^2x^2z^2\sin\theta + 4ik^2y^2z^2\sin\theta - 6ik^2z^4\sin\theta + \\
+4ie^{ik(z\cos\theta+x\sin\theta)}k^2z^4\sin\theta + 16kx^2z\sin 2\theta - \\
-56e^{ik(z\cos\theta+x\sin\theta)}kx^2z\sin 2\theta - 4k^3x^4z\sin 2\theta - 16ky^2z\sin 2\theta - \\
-32e^{ik(z\cos\theta+x\sin\theta)}ky^2z\sin 2\theta - 12k^3x^2y^2z\sin 2\theta + 16kz^3\sin 2\theta + \\
+24e^{ik(z\cos\theta+x\sin\theta)}kz^3\sin 2\theta - 4k^3y^2z^3\sin 2\theta + 4k^3z^5\sin 2\theta - 8ix^2\sin 3\theta + \\
+8ie^{ik(z\cos\theta+x\sin\theta)}x^2\sin 3\theta + ik^2x^4\sin 3\theta - \\
-10ie^{ik(z\cos\theta+x\sin\theta)}k^2x^4\sin 3\theta - 4ik^2x^2y^2\sin 3\theta + 8iz^2\sin 3\theta - \\
-8ie^{ik(z\cos\theta+x\sin\theta)}z^2\sin 3\theta + 18ik^2x^2z^2\sin 3\theta + \\
+12ie^{ik(z\cos\theta+x\sin\theta)}k^2x^2z^2\sin 3\theta + 4ik^2y^2z^2\sin 3\theta - 7ik^2z^4\sin 3\theta + \\
+6ie^{ik(z\cos\theta+x\sin\theta)}k^2z^4\sin 3\theta + 12e^{ik(z\cos\theta+x\sin\theta)}kx^2z\sin 4\theta + \\
+2k^3x^4z\sin 4\theta + 6k^3x^2y^2z\sin 4\theta - 4e^{ik(z\cos\theta+x\sin\theta)}kz^3\sin 4\theta - 12k^3x^2z^3\sin 4\theta - \\
-2k^3y^2z^3\sin 4\theta + 2k^3z^5\sin 4\theta - ik^2x^4\sin 5\theta + 2ie^{ik(z\cos\theta+x\sin\theta)}k^2x^4\sin 5\theta + \\
+6ik^2x^2z^2\sin 5\theta - 12ie^{ik(z\cos\theta+x\sin\theta)}k^2x^2z^2\sin 5\theta - ik^2z^4\sin 5\theta + 2ie^{ik(z\cos\theta+x\sin\theta)}k^2z^4\sin 5\theta]
\end{gathered}
\tag{25}
$$

$$
\begin{gathered}
j_{\times,y}^{XZ} = \frac{1}{32\sqrt{2}k(z\cos\theta + x\sin\theta)^4} e^{-ikt}y[-128ie^{ik(z\cos\theta+x\sin\theta)}z + 16ik^2x^2z + 16ik^2z^3 + \\
+2k(k^2x^4 + x^2(8 + 8eik(z\cos\theta + x\sin\theta) - 6k^2z^2) - z^2(8 + 40e^{ik(z\cos\theta+x\sin\theta)} + \\
+7k^2z^2))\cos\theta + 16iz(-4 + 4e^{iz(z\cos\theta+x\sin\theta)} + k^2(-x^2+z^2))\cos 2\theta - \\
-16kx^2\cos 3\theta - 16e^{ik(z\cos\theta+x\sin\theta)}kx^2\cos 3\theta - 3k^3x^4\cos 3\theta + 16kz^2\cos 3\theta + 16e^{ik(z\cos\theta+} \\
x\sin\theta)kz^2\cos 3\theta + 18k^3x^2z^2\cos 3\theta - 3k^3z^4\cos 3\theta + k^3x^4\cos 5\theta - 6k^3x^2z^2\cos 5\theta + k^3z^4\cos 5\theta - \\
-32kxz\sin\theta - 96e^ik(z\cos\theta + x\sin\theta)kxz\sin\theta - 16k^3x^3z\sin\theta - 16k^3xz^3\sin\theta - 64ix\sin 2\theta + \\
+64ie^{ik(z\cos\theta+x\sin\theta)}x\sin 2\theta + 32ik^2xz^2\sin 2\theta + 32kxz\sin 3\theta + 32e^{ik(z\cos\theta+} \\
+x\sin\theta)kxz\sin 3\theta + 12k^3x^3z\sin 3\theta - 12k^3xz^3\sin 3\theta - 4k^3x^3z\sin 5\theta + 4k^3xz^3\sin 5\theta]
\end{gathered}
\tag{26}
$$

$$
\begin{gathered}
j_{+,y}^{YZ} = \frac{1}{8\sqrt{2}k(z\cos\theta + y\sin\theta)^3} e^{-ikt}x[-16i + 16ie^{ik(z\cos\theta+y\sin\theta)} - 4ik^2y^2 + \\
+3ie^{ik(z\cos\theta+y\sin\theta)}k^2y^2 - 4ik^2z^2 + ie^{ik(z\cos\theta+y\sin\theta)}k^2z^2 + \\
+kz(2 + 14e^{ik(z\cos\theta+y\sin\theta)} + 3k^2(y^2+z^2))\cos\theta - \\
-4ik^2(-1 + e^{ik(z\cos\theta+y\sin\theta)}y^2 + z^2)\cos 2\theta - 2kz\cos 3\theta + \\
+2e^{ik(z\cos\theta+y\sin\theta)}kz\cos 3\theta - 3k^3y^2z\cos 3\theta + k^3z^3\cos 3\theta + \\
+ie^{ik(z\cos\theta+y\sin\theta)}k^2y^2\cos 4\theta - ie^{ik(z\cos\theta+y\sin\theta)}k^2z^2\cos 4\theta + \\
+6ky\sin\theta + 10e^{ik(z\cos\theta+y\sin\theta)}ky\sin\theta + 3k^3y^3\sin\theta + 3k^3yz^2\sin\theta - \\
-8ik^2yz\sin 2\theta + 4ie^{ik(z\cos\theta+y\sin\theta)}k^2yz\sin 2\theta - 2ky\sin 3\theta + \\
+2e^{ik(z\cos\theta+y\sin\theta)}ky\sin 3\theta - k^3y^3\sin 3\theta + 3k^3yz^2\sin 3\theta - 2ie^{ik(z\cos\theta+y\sin\theta)}k^2yz\sin 4\theta]
\end{gathered}
\tag{27}
$$

$$
\begin{gathered}
j_{\times,y}^{YZ} = \frac{1}{2\sqrt{2}k(z\cos\theta + y\sin\theta)^3} e^{-ikt}[k^3yz^3(\cos\theta)^4 - k^2z^2(\cos\theta)^3(2iy + k(-3y^2+z^2)\sin\theta) - \\
-z\sin\theta(-2i + ky\sin\theta)(2 - 2e^{ik(z\cos\theta+y\sin\theta)} + 2ie^{ik(z\cos\theta+y\sin\theta)}ky\sin\theta + k^2y^2(\sin\theta)^2) + \\
+kz(\cos\theta)^2(4e^{ik(z\cos\theta+y\sin\theta)}y - 2ik(2y^2 + (2y^2 + (-1 + e^{ik(z\cos\theta+y\sin\theta)}z^2)\sin\theta + \\
+3k^2y(y^2 - z^2)(\sin\theta)^2) + \cos\theta(4i(-1 + e^{ik(z\cos\theta+y\sin\theta)})y - \\
-2k(z^2 + e^{ik(z\cos\theta+y\sin\theta)}(-2y^2+z^2))\sin\theta - 2ik^2y(y^2 + 2(-1 + e^{ik(z\cos\theta+y\sin\theta)})z^2)(\sin\theta)^2 + \\
+k^3y^2(y^2 - 3z^2)(\sin\theta)^2)]
\end{gathered}
\tag{28}
$$

By Dr. Camilo García-Cely (IFIC)

INDEX

The inspiral of two compact binaries

- As an example, we have assumed an **inspiral of two compact binaries**, where two compact neutron stars or black holes are rotating around the mass center of the system in an inspiral dynamic system which will coalesce in a unique large object emitting GWs.

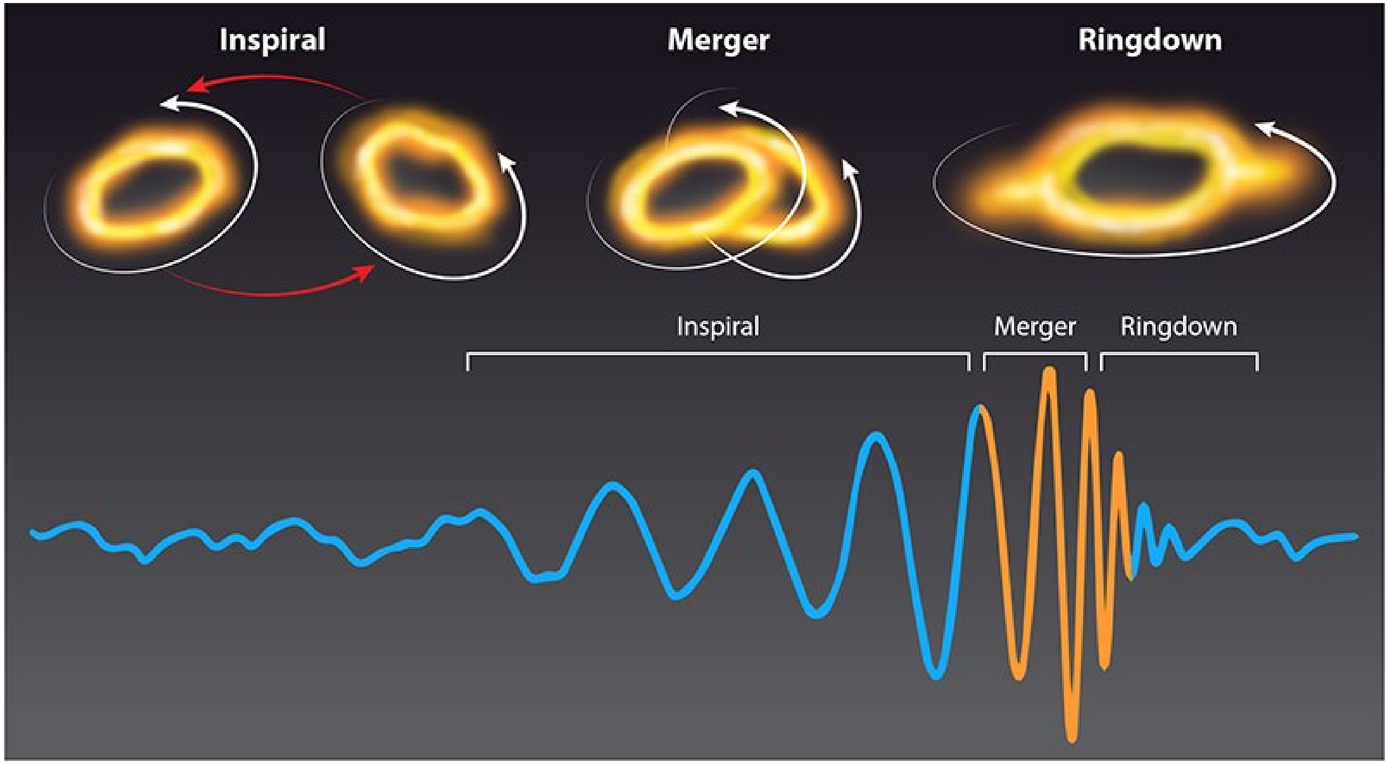

The inspiral of two compact binaries

- The equivalent electric current density of the GW is expressed as follows

$$\vec{J}_{GW}(\vec{r}) = \frac{1}{\mu_0} B_{0_z} \left(h_+ \vec{J}_+(\vec{r}) + h_\times \vec{J}_\times(\vec{r}) \right)$$

where for this case we have (Maggiore, Gravitational Waves: Volume 1: Theory and Experiments):

XZ plane: $$h_+ = -\Lambda \frac{1+\cos^2\theta}{2} \; ; \; h_\times = j\,\Lambda\,\cos\theta$$

YZ plane: $$h_+ = \Lambda \frac{1+\cos^2\theta}{2} \; ; \; h_\times = -j\,\Lambda\,\cos\theta$$

where θ is the spherical elevation angle, and the amplitude of the GW is given by

$$\Lambda = \frac{1}{2^{1/3}} \frac{R_c}{r} \left(\frac{R_c\,\omega}{c} \right)^{2/3}$$

R_c is the **Schwarzschild radius** associated to the chirp mass, and M_c is the **chirp mass**

$$R_c = \frac{2\,G\,M_c}{c^2} \qquad\qquad M_c = \frac{(m_1\,m_2)^{3/5}}{(m_1 + m_2)^{1/5}}$$

INDEX

The cubic resonator

- In this cumbersome scenario we decided to use a **cubic resonator** with three degenerated modes that can be **independently** and **simultaneously** detected with three coaxial antennas placed in orthogonal directions.
- The homogeneous magnetostatic field B is oriented in the Z axis.
- Electric (up) and magnetic (down) field distributions of the three degenerate modes.

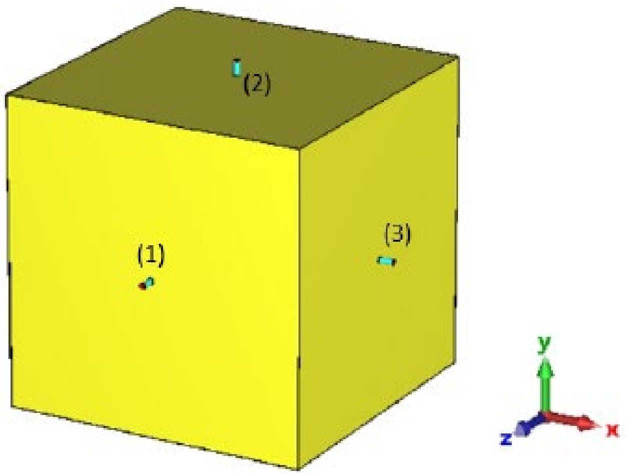

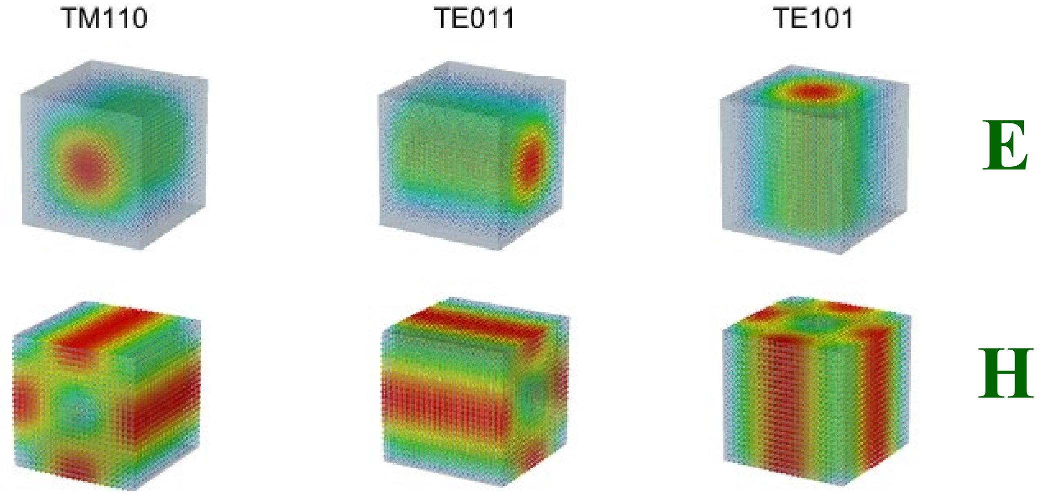

The cubic resonator

- In order to explore different frequencies we have studied three different cavities (a is the edge length of the cube):

$$f_{TE_{101}} = f_{TE_{011}} = f_{TM_{110}} = \frac{c}{2\,a}$$

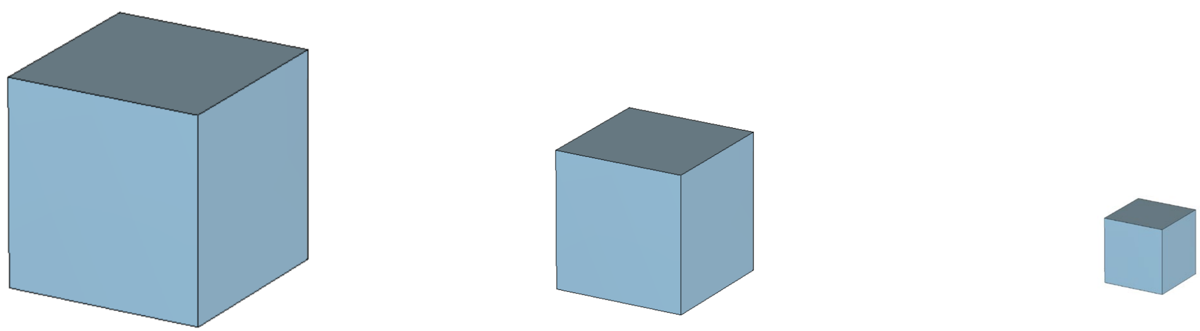

CAVITY C1: 100 MHz **CAVITY C2: 1 GHz** **CAVITY C3: 10 GHz**

INDEX

Application of the BI-RME 3D formulation

- **BI-RME 3D = Boundary Integral - Resonant Mode Expansion**
- The expressions of the electric and magnetic fields existing in the cavity excited by the time-harmonic electric $\vec{J}$ and magnetic $\vec{M}$ current densities are:

$$\vec{E}(\vec{r}) = \frac{\eta}{jk}\nabla\int_V g^e(\vec{r},\vec{r}')\,\nabla'\cdot\vec{J}(\vec{r}')\,dV' - jk\eta\int_V \vec{\mathbf{G}}^{\mathrm{A}}(\vec{r},\vec{r}')\cdot\vec{J}(\vec{r}')\,dV' - $$
$$-\int_S \nabla\times\vec{\mathbf{G}}^{\mathrm{F}}(\vec{r},\vec{r}')\cdot\vec{M}(\vec{r}')\,dS' + \frac{1}{2}\vec{n}\times\vec{M}$$

$$\vec{H}(\vec{r}) = \frac{1}{jk\eta}\nabla_s\int_S g^m(\vec{r},\vec{r}')\,\nabla'\cdot\vec{M}(\vec{r}')\,dS' - \frac{jk}{\eta}\int_S \vec{\mathbf{G}}^{\mathrm{F}}(\vec{r},\vec{r}')\cdot\vec{M}(\vec{r}')\,dS' + $$
$$+\int_V \nabla\times\vec{\mathbf{G}}^{\mathrm{A}}(\vec{r},\vec{r}')\cdot\vec{J}(\vec{r}')\,dV'$$

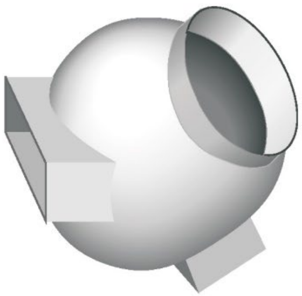

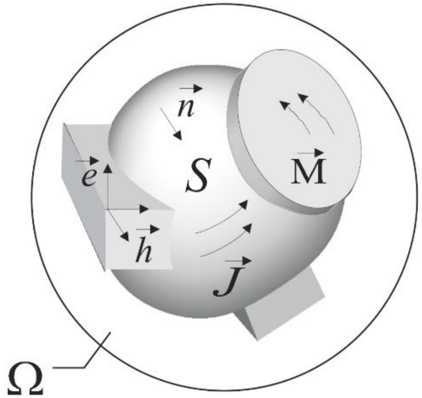

Application of the BI-RME 3D formulation

- We have used the BI-RME 3D technique for the efficient and accurate electromagnetic analysis of the cavity excited by the GWs.
- This is the equivalent network for a three ports structure driven by three current sources:

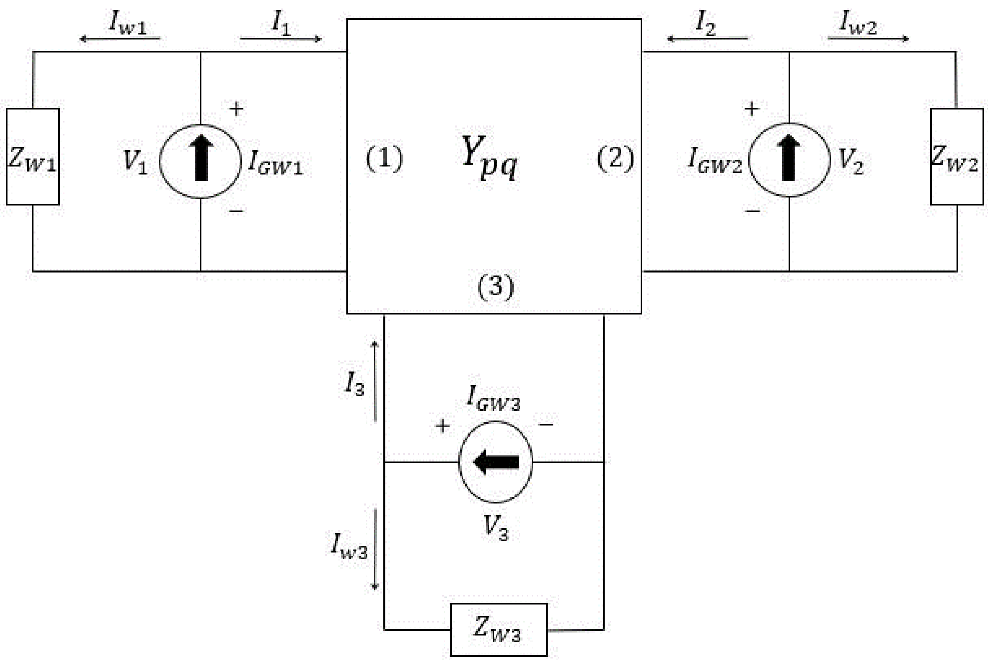

$$\begin{pmatrix} I_1 \\ I_2 \\ I_3 \end{pmatrix} = \begin{pmatrix} Y_{11} & Y_{12} & Y_{13} \\ Y_{21} & Y_{22} & Y_{23} \\ Y_{31} & Y_{32} & Y_{33} \end{pmatrix} \cdot \begin{pmatrix} V_1 \\ V_2 \\ V_3 \end{pmatrix}$$

Ohmic losses (Joule effect)

$$\boxed{\kappa_m \approx k_m \left(1 - \frac{1}{2\,Q_m}\right) + j\,\frac{k_m}{2\,Q_m}}$$

$$I_{GW_i} = \sum_{m=1}^{M} \frac{\kappa_m}{k^2 - \kappa_m^2} \underbrace{\left(\int_{S(i)} \vec{H}_m(\vec{r}) \cdot \vec{h}_1^{(i)}(\vec{r})\, dS \right)}_{COUPLING:CAV-PORT} \underbrace{\left(\int_V \vec{E}_m(\vec{r}\,') \cdot \vec{J}_{GW}(\vec{r}\,')\, dV' \right)}_{COUPLING:GW-CAV}$$

$$i \in \{1, 2, 3, \ldots P\}$$

Application of the BI-RME 3D formulation

- Finally we can solve the linear system considering the inter-coupling among the three ports

$$I_{GW_i} = I_i + I_{W_i}\,;\, V_i = Z_{W_i} I_{W_i} \Longrightarrow I_i = I_{GW_i} - I_{W_i} = I_{GW_i} - Y_{W_i} V_i$$

$$i \in \{1, 2, 3\}$$

$$\begin{pmatrix} I_{GW_1} \\ I_{GW_2} \\ I_{GW_3} \end{pmatrix} = \begin{pmatrix} Y_{11} + Y_{W_1} & Y_{12} & Y_{13} \\ Y_{21} & Y_{22} + Y_{W_2} & Y_{23} \\ Y_{31} & Y_{32} & Y_{33} + Y_{W_3} \end{pmatrix} \cdot \begin{pmatrix} V_1 \\ V_2 \\ V_3 \end{pmatrix}$$

in order to obtain the power extracted in each port as well as the voltage amplitude measured (magnitude and phase):

$$P_{W_i} = \frac{1}{2} Re(V_i\, I^*_{W_i}) = \frac{1}{2} Re(Y^*_{W_i})\, |V_i|^2$$

$$v_i = \sqrt{\frac{\ln{(r_o/r_i)}}{2\,\pi}}\, V_i$$

INDEX

Numerical results and discussion

- Characteristic of the three cubic cavities:

	CAVITY 1	CAVITY 2	CAVITY 3
a (mm)	2119.85	211.98	21.19
Q_{TE101}	$6.27 \cdot 10^5$	$1.98 \cdot 10^5$	$6.25 \cdot 10^4$
Q_{TE011}	$6.27 \cdot 10^5$	$1.98 \cdot 10^5$	$6.25 \cdot 10^4$
Q_{TM110}	$6.27 \cdot 10^5$	$1.98 \cdot 10^5$	$6.25 \cdot 10^4$
r_i (mm)	7.00	0.0635	0.0635
r_o (mm)	16.00	0.211	0.211
ε_r	1.00	2.08	2.08
d (mm)	32.80	5.30	0.21

Table 1. Characteristics of the three cubic cavities and their coaxial probes.

- d is the length of the coaxial probes for critical coupling regime
- coaxial connectors: BNC for C1, and SMA for C2 and C3
- simulations: Cu at cryogenic temperature (1 K), $\sigma = 2 \cdot 10^9$ S/m

Numerical results and discussion

- For the calculations we have used realistic magnets:

Cavity	V (L)	Magnet	B_0 (T)	T_{phys} (mK)	T_{sys} (K)
C1	9526.1056	KLASH [52]	0.6	4500	8
C2	9.5243	CAPP [53]	12	30	1
C3	0.0095	CAPP [53]	12	30	1

Table 4. Characteristics of the magnets and parameters for the data acquisi

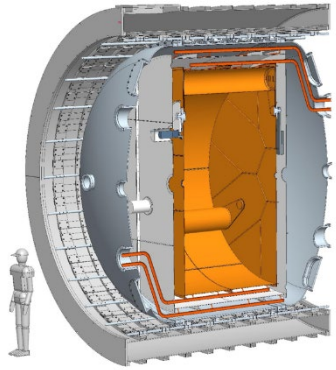

INFN-Frascati
KLASH

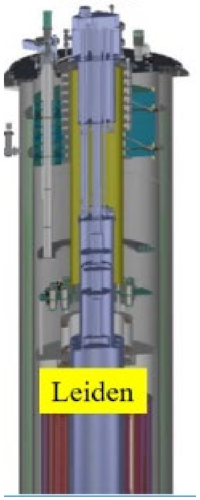

- The form factor accounts for the coupling between the GW and the resonant modes as a function of the GW incidence angle θ in the XZ, YZ and XY planes :

$$\tilde{\eta}_{m_{+,\times}} = \frac{\left| \int_V \vec{E}_m(\vec{r}) \cdot \vec{J}_{+,\times}(\vec{r})\, dV \right|}{V^{1/2} \left| \int_V \vec{E}_m(\vec{r}) \cdot \vec{E}_m(\vec{r})\, dV \right|^{1/2}}$$

Numerical results and discussion

CAVITY C1: 100 MHz

x polarization

+ polarization

XZ plane

YZ plane

XY plane

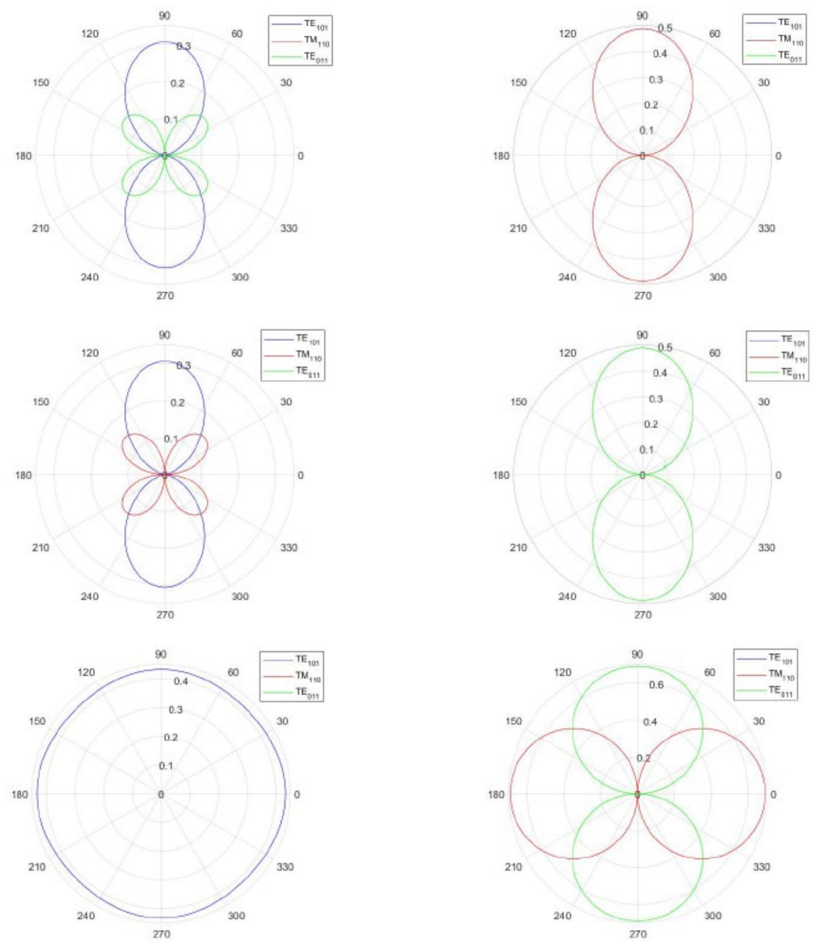

Figure 4. Form factor $\tilde{\eta}_{m_{+,\times}}$ between the GW and the three degenerated resonant modes as a function of the GW incidence angular direction for the cavity C1 (f = 100 MHz). The polar angle is expressed in degrees. Some curves cannot be seen because the form factor is negligible compared to the rest of the results. Left: cross polarization; Right: plus polarization. Up: GW incidence in the XZ plane; Center: GW incidence in the YZ plane; Down: GW incidence in the XY plane.

Numerical results and discussion

CAVITY C2: 1 GHz

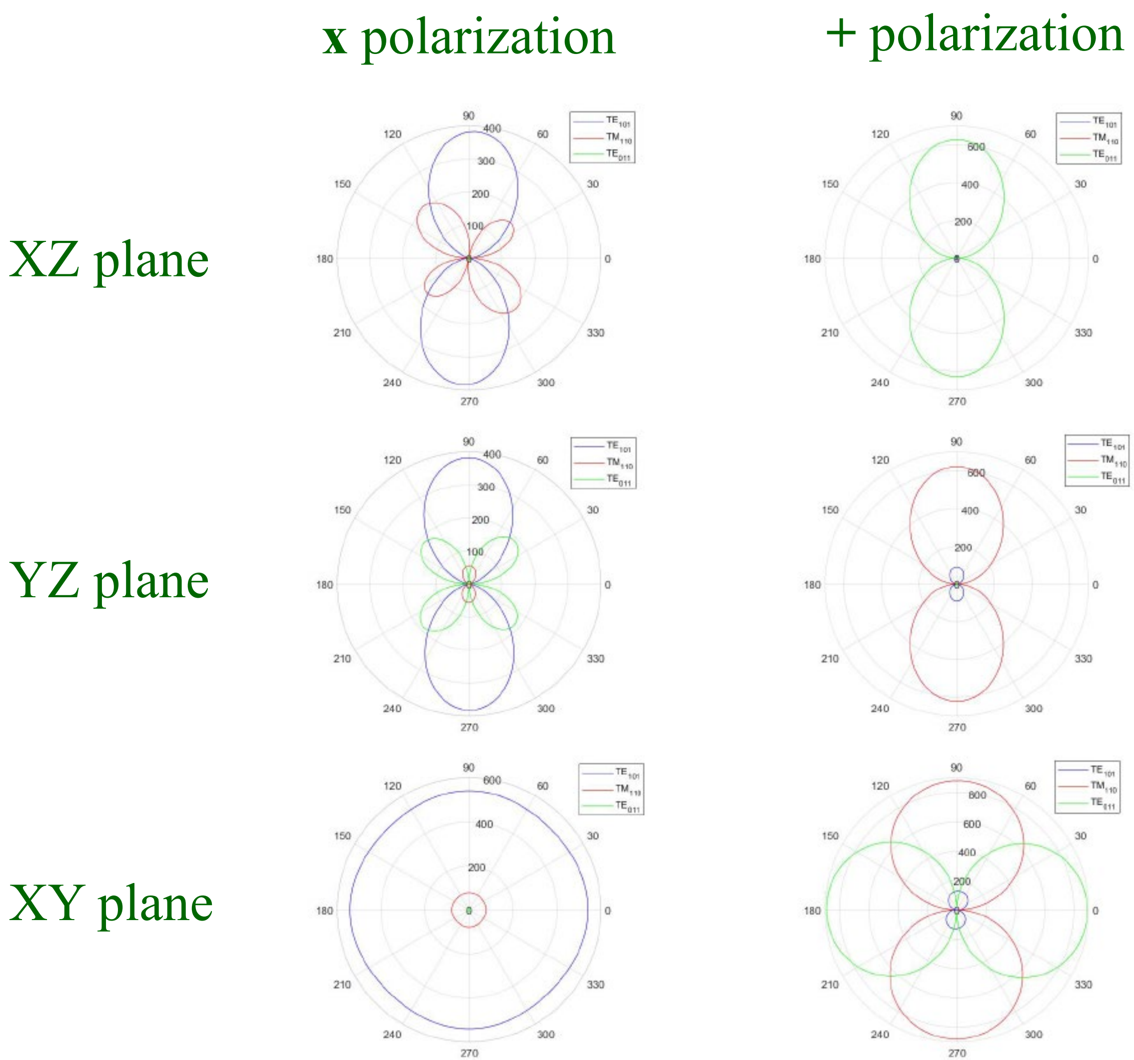

Figure 5. Form factor $\tilde{\eta}_{m_{+,\times}}$ between the GW and the three degenerated resonant modes as a function of the GW incidence angular direction for the cavity C2 ($f = 1$ GHz). The polar angle is expressed in degrees. Some curves cannot be seen because the form factor is negligible compared to the rest of the results. Left: cross polarization; Right: plus polarization. Up: GW incidence in the XZ plane; Center: GW incidence in the YZ plane; Down: GW incidence in the XY plane.

Numerical results and discussion

CAVITY C3: 10 GHz

x polarization + polarization

XZ plane

YZ plane

XY plane

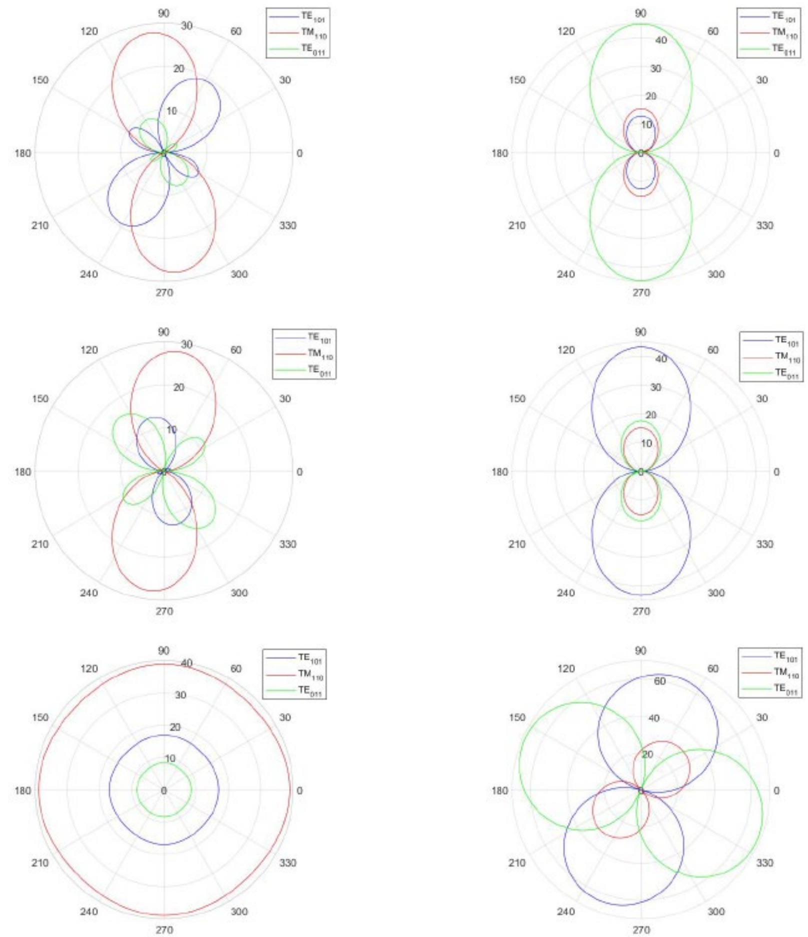

Figure 6. Form factor $\tilde{\eta}_{m_{+,\times}}$ between the GW and the three degenerated resonant modes as a function of the GW incidence angular direction for the cavity C3 ($f = 10$ GHz). The polar angle is expressed in degrees. Some curves cannot be seen because the form factor is negligible compared to the rest of the results. Left: cross polarization; Right: plus polarization. Up: GW incidence in the XZ plane; Center: GW incidence in the YZ plane; Down: GW incidence in the XY plane.

- **Sensitivity analysis**:

- Power excited in each coaxial port:

$$P_{W_{i_{\times,+}}} = \frac{1}{2}\left|h_{\times,+}\right|^2 \frac{B_0^2\, V}{\mu_0^2} \frac{\mathrm{Re}(Y_{W_i})}{\left|Y_{W_i} + Y_{ii}\right|^2} \left| \sum_{m=1}^{M} \frac{\kappa_m}{k^2 - \kappa_m^2}\, \tilde{\eta}_{m+,\times} \int_{S(i)} \vec{H}_m(\vec{r}) \cdot \vec{h}_1^{(i)}(\vec{r})\, dS \right|^2$$

- The Dick radiometer equation for white noise provides the noise in the port i:

$$P_{N_i} = k_B\, T_{sys_i} \sqrt{\frac{\Delta f}{\Delta t}}$$

where k_B is the Boltzmann constant, $T_{sys,I}$ is the noise temperature of the system at port i, Δf is the detection bandwidth, and Δt is the detection time.

Numerical results and discussion

- The amplitude of the GW at each port for each polarization is obtained by means:

$$|h_{i_{\times,+}}| = \left(\frac{2\,(S/N)\,k_B\,T_{sys_i}}{\mathrm{Re}(Y_{W_i})}\right)^{1/2} \left(\frac{\Delta f}{\Delta t}\right)^{1/4} \frac{\mu_0}{B_0\,V^{\frac{1}{2}}} \frac{|Y_{W_i}+Y_{ii}|}{\left|\sum_{m=1}^{M} \frac{\kappa_m}{k^2-\kappa_m^2}\,\tilde{\eta}_{m_{\times,+}} \int_{S(i)} \vec{H}_m(\vec{r})\cdot\vec{h}_1^{(i)}(\vec{r})\,dS\right|}$$

- Signal/Noise ratio: $S/N = P_{Wi}/P_{Ni} = 3$ for the numerical simulations.

- Finally we present results of the power and voltage (magnitude and phase) for **C1 (f=100 MHz)** because of brevity.

Numerical results and discussion

CAVITY C1: 100 MHz

sensitivity analysis

x polarization | + polarization

XZ plane

YZ plane

XY plane

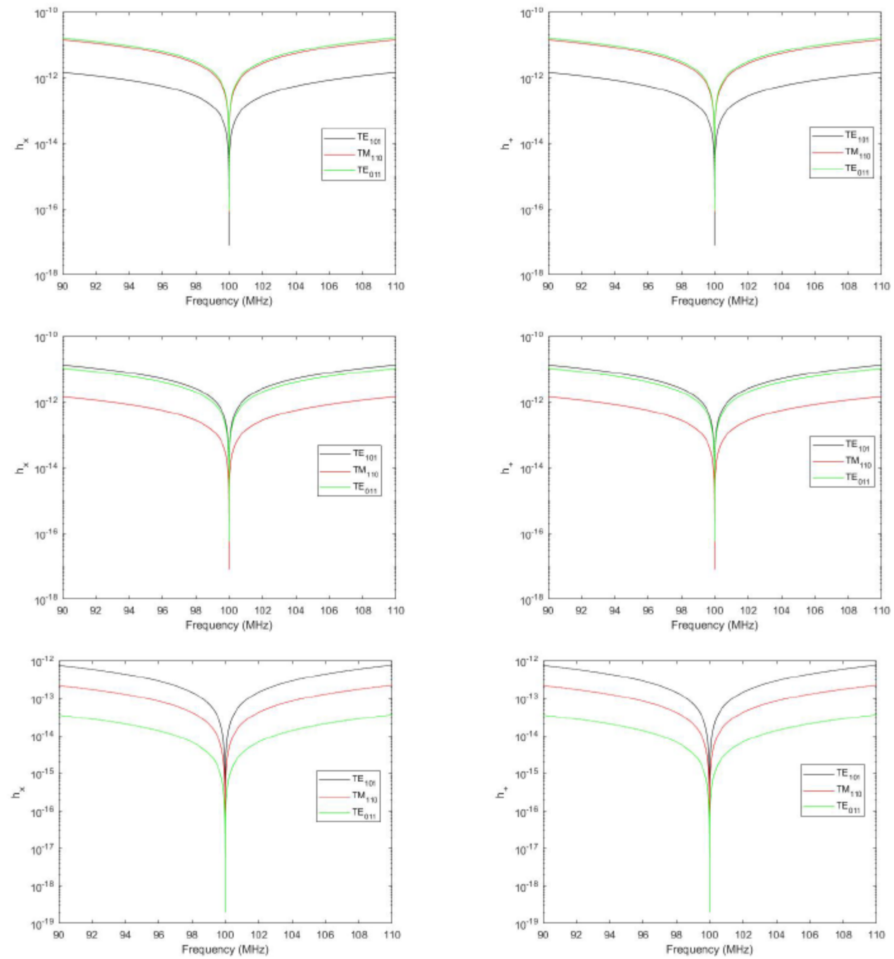

Figure 7. GWs amplitudes $h_\times$ and h_+ as a function of frequency in the three coaxial probes of the cavity C1 ($f = 100$ MHz). Magnetostatic field: $B_0 = 0.6$ T; signal-to-noise ratio: $S/N = 3$; temperature of the system: $T_{sys} = 8$ K; frequency detection bandwidth: $\Delta f = 5$ KHz; detection time: $\Delta t = 1$ ms. Left: cross polarization; Right: plus polarization. Up: GW incidence in the XZ plane; Center: GW incidence in the YZ plane; Down: GW incidence in the XY plane.

CAVITY C1: 100 MHz

detected power

x polarization

+ polarization

XZ plane

YZ plane

XY plane

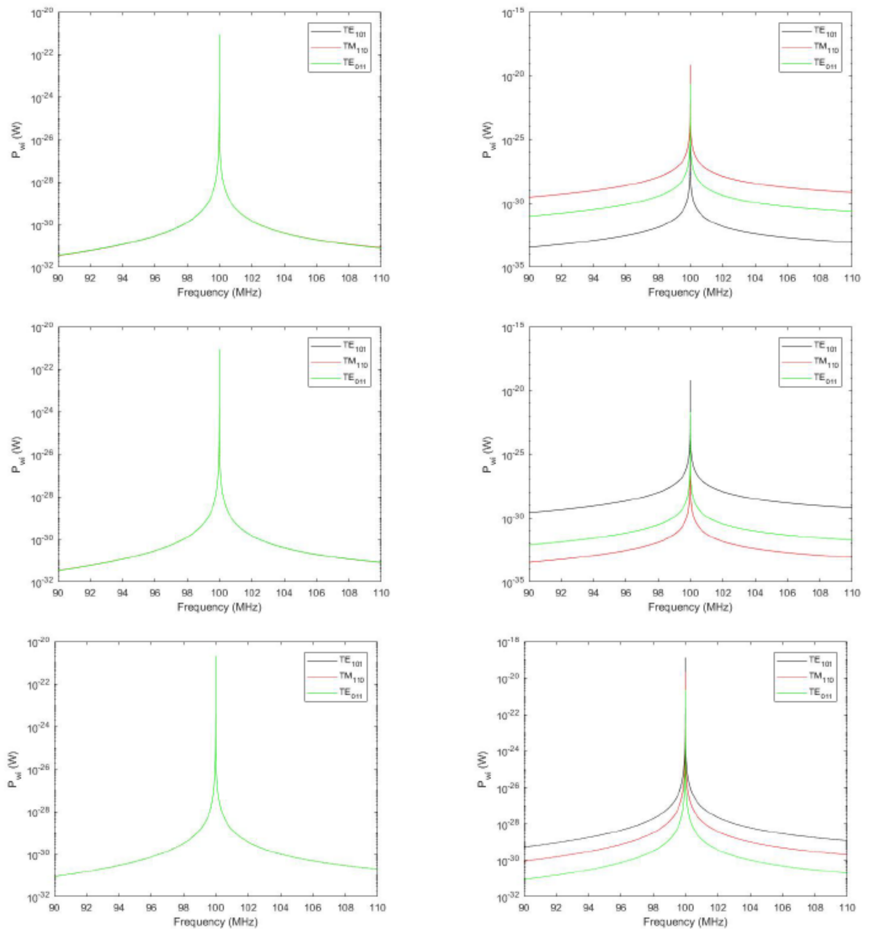

Figure 10. Detected power of the GWs as a function of frequency in the three coaxial probes of the cavity C1 ($f = 100$ MHz), related to the GW amplitudes obtained in figure 7. Magnetostatic field: $B_0 = 0.6$ T; signal-to-noise ratio: $S/N = 3$; temperature of the system: $T_{sys} = 8$ K; frequency detection bandwidth: $\Delta f = 5$ KHz; detection time: $\Delta t = 1$ ms. Left: cross polarization; Right: plus polarization. Up: GW incidence in the XZ plane; Center: GW incidence in the YZ plane; Down: GW incidence in the XY plane.

Numerical results and discussion

CAVITY C1: 100 MHz

magnitude of the voltage

x polarization

+ polarization

XZ plane

YZ plane

XY plane

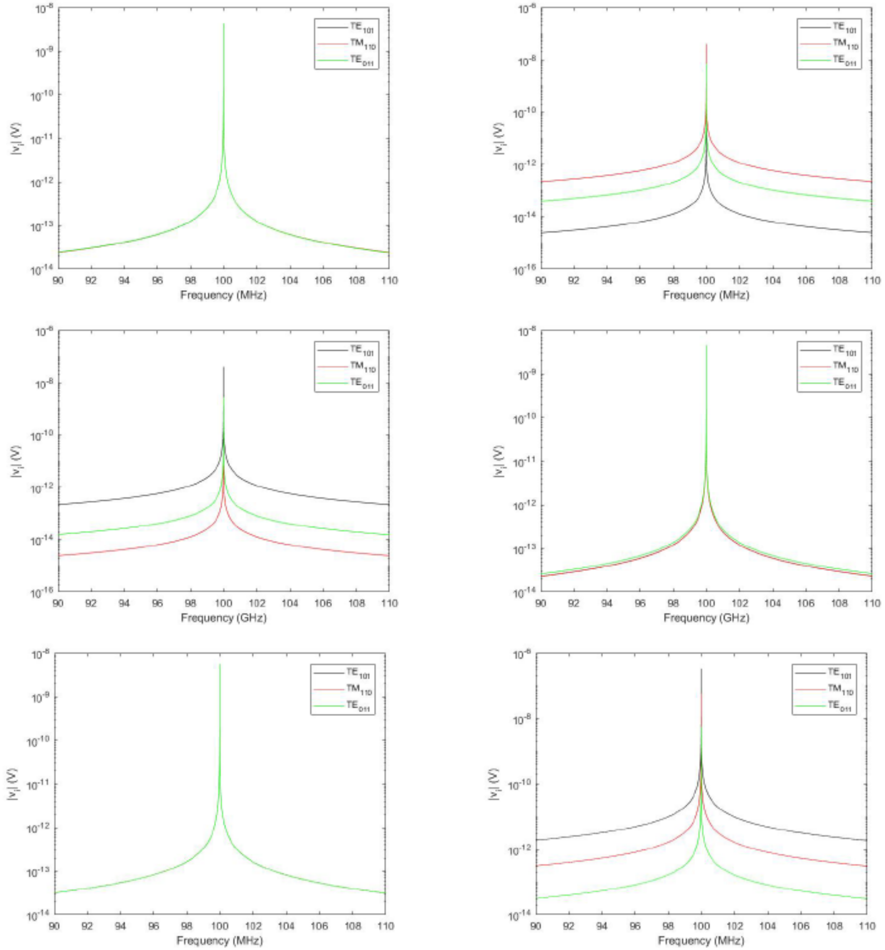

Figure 11. Magnitude of the detected voltages $|v_i|$ as a function of frequency in the three coaxial probes of the cavity C1 ($f = 100$ MHz). Magnetostatic field: $B_0 = 0.6$ T; signal-to-noise ratio: $S/N = 3$; temperature of the system: $T_{sys} = 1$ K; frequency detection bandwidth: $\Delta f = 5$ KHz; detection time: $\Delta t = 1$ ms. Left: cross polarization; Right: plus polarization. Up: GW incidence in the XZ plane; Center: GW incidence in the YZ plane; Down: GW incidence in the XY plane.

Numerical results and discussion

CAVITY C1: 100 MHz

phase of the voltage

x polarization + polarization

XZ plane

YZ plane

XY plane

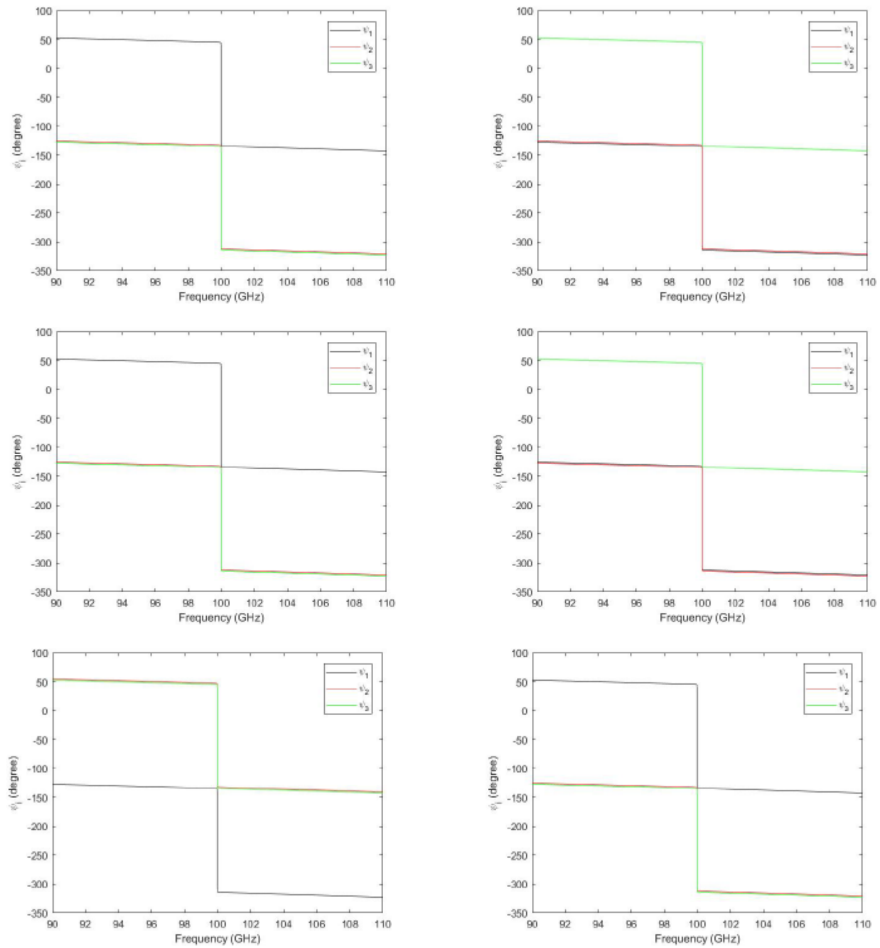

Figure 12. Phase of the detected voltages ψ_i as a function of frequency in the three coaxial probes of the cavity C1 ($f = 100$ MHz). Magnetostatic field: $B_0 = 0.6$ T; signal-to-noise ratio: $S/N = 3$; temperature of the system: $T_{sys} = 8$ K; frequency detection bandwidth: $\Delta f = 5$ KHz; detection time: $\Delta t = 1$ ms. Left: cross polarization; Right: plus polarization. Up: GW incidence in the XZ plane; Center: GW incidence in the YZ plane; Down: GW incidence in the XY plane.

INDEX

Conclusions and future research lines

- **Conclusions:**

- We have presented the electromagnetic analysis of a cubic cavity for the detection of GWs at microwave frequencies.
- Three different resonators have been studied at 100 MHz, 1 GHz and 10 GHz.
- Three coaxial antennas have been used for the simultaneous detection of the three degenerate modes TE_{101}, TE_{011} and TM_{110}.
- These coaxial probes have been placed in three orthogonal planes of the cubic cavity, and they have been designed for critical coupling regime.
- The BI-RME 3D technique has been used for an efficient and accurate electromagnetic analysis.
- The GWs excitation of the cavity has been studied in terms of a volumetric current density considering the two polarizations “plus” and “cross”.
- We have analyzed the incidence of the GW as a function of the incidence angle of the GW wavenumber vector in three perpendicular planes.
- Preliminary results for the sensitivity analysis have been presented.

Conclusions and future research lines

- **Future research lines:**

➢ Study of the **arbitrary 3D incidence** of the GW

➢ Frequency response of the system has to be extended considering that the GW source of a binary system has a **chirp excitation frequency spectrum**

➢ Analysis of **cylindrical, spherical**, etc cavities

➢ Both amplitude and phase of the voltage measured at each coaxial probe has been calculated which is fundamental for **interferometry analysis** of GWs

➢ Analysis of the **babyIAXO haloscopes** (dark matter axions search) for GWs detection:

S. Ahyoune et al, "A Proposal for a Low-Frequency Axion Search in the 1–2 μeV Range and Below with the BabyIAXO Magnet", Annalen der Physik, 2300326, pp. 1-23, 2023

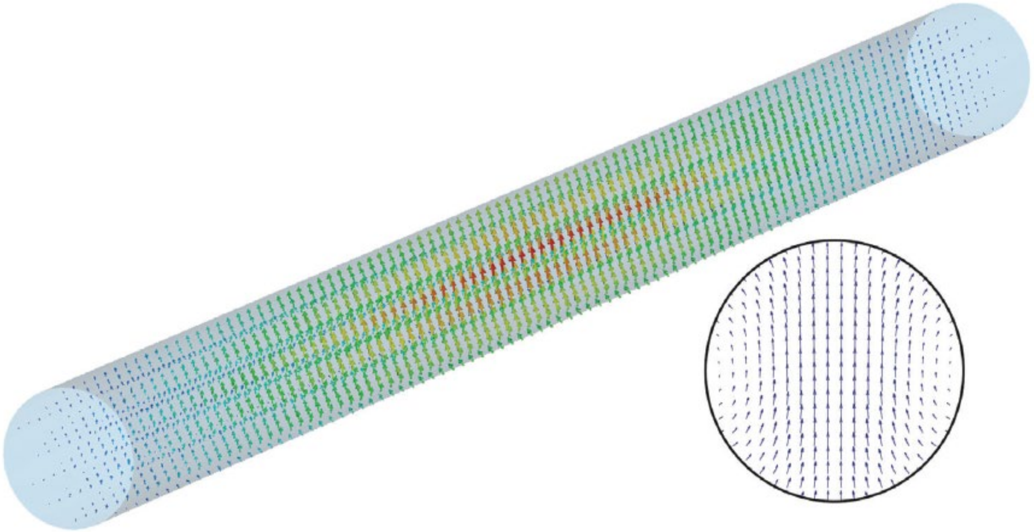

Thanks a lot for your attention. We are open to cooperate with all of you.

benito.gimeno@uv.es

arXiv:2312.02270v1

The inspiral of two compact binaries

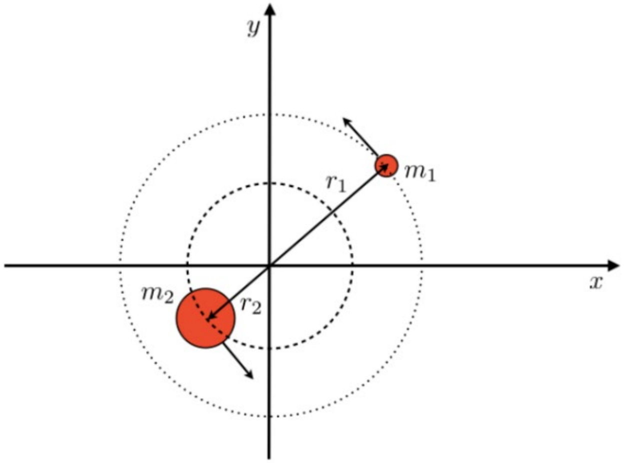

- Example:
  - two black holes
  - $m_1 = m_2 = 1.4\ M_\odot$ ➡ $M_c = 1.2\ M_\odot$
  - coalescence time = 17 minutes
  - frequency = from 10 Hz up to 1 kHz

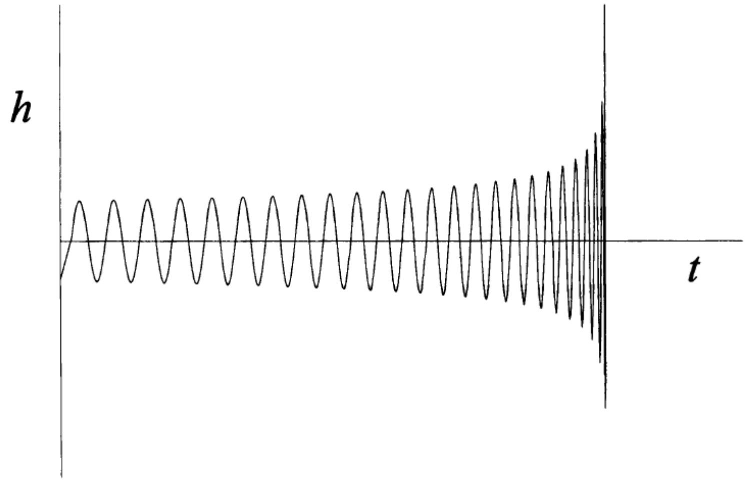

Fig. 4.2 The time evolution of the GW amplitude in the inspiral phase of a binary system.

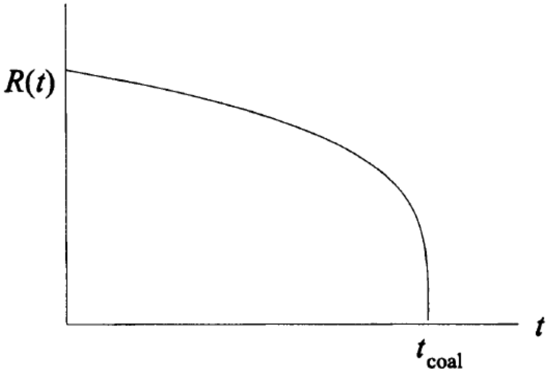

Fig. 4.1 The evolution of the separation $R(t)$ between the two bodies, in the lowest-order Newtonian approximation.

Numerical results and discussion

x polarization + polarization

CAVITY C1: 100 MHz

XZ plane

detected power

YZ plane

XY plane

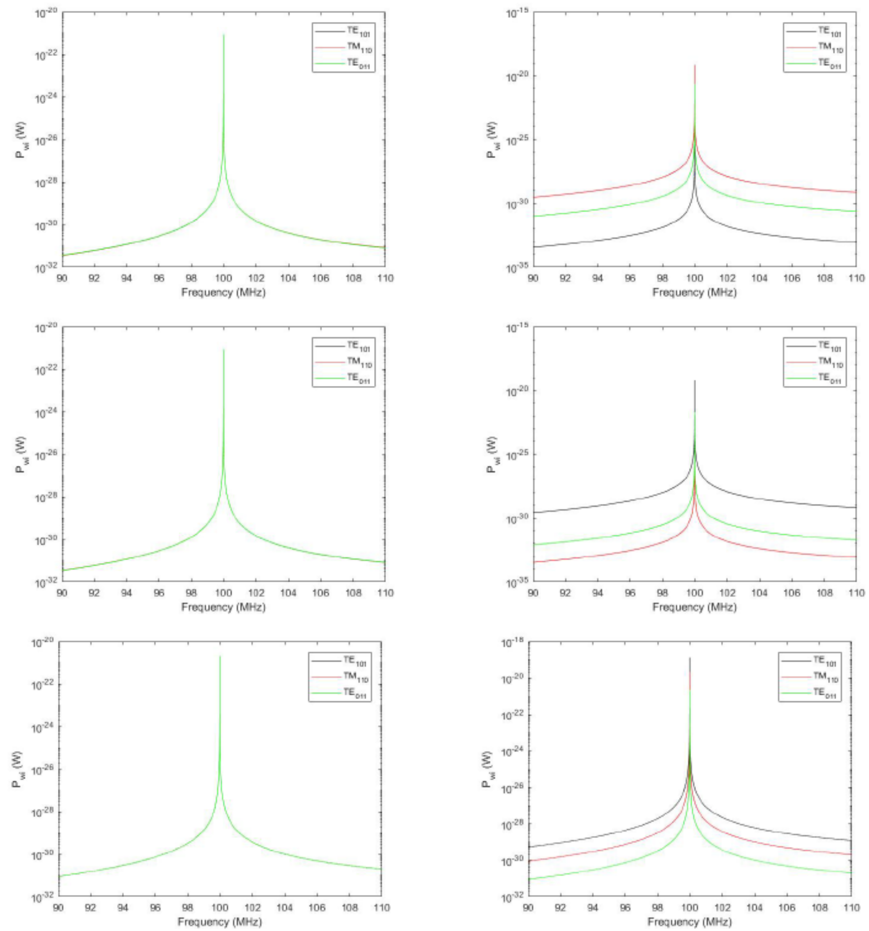

Figure 10. Detected power of the GWs as a function of frequency in the three coaxial probes of the cavity C1 ($f = 100$ MHz), related to the GW amplitudes obtained in figure 7. Magnetostatic field: $B_0 = 0.6$ T; signal-to-noise ratio: $S/N = 3$; temperature of the system: $T_{sys} = 8$ K; frequency detection bandwidth: $\Delta f = 5$ KHz; detection time: $\Delta t = 1$ ms. Left: cross polarization; Right: plus polarization. Up: GW incidence in the XZ plane; Center: GW incidence in the YZ plane; Down: GW incidence in the XY plane.

How many photons are detecting ?

$P_w = 10^{-20}$ W = 10^{-20} J/s

Energy of a photon: $E_f = h f$

$E_f = 6.6\ 10^{-34} * 100\ 10^6 = 6.6\ 10^{-26}$ J

Number of photons per second =

$=10^{-20}$ J/E_f = 1.5 10^5 photons